Dimensionality Dependence of Optical Properties and Quantum Confinement Effects of Hydrogenated Silicon Nanostructures

Man-Fai Ng and R. Q. Zhang*

Center of Super-Diamond and Advanced Films (COSDAF) and Department of Physics and Materials Science, City University of Hong Kong, 83 Tat Chee Avenue, Kowloon, Hong Kong SAR, China

Received: June 22, 2006; In Final Form: August 25, 2006

The excited state properties of linear, planar, and spherical hydrogenated silicon nanostructures are studied systematically with use of a time-dependent Hartree−Fock (TDHF) approach with a semiempirical Hamiltonian. The calculated optical gaps decrease significantly from linear, planar, to spherical silicon structures, showing that the optical gap is dimensionality dependent and hence it can be varied by solely managing the shape of the nanostructures. Remarkably, the calculated exciton sizes of the lowest dipole-allowed excited states for both silicon chains and planes are ∼26 Å, revealing that the quantum confinement effect should be significantly enhanced when the sizes of silicon nanostructures are smaller than this value but not dependent on the dimensionality. A similar trend is also observed for hydrogenated silicon spherical clusters.

Introduction

Hydrogenated silicon nanostructures have drawn increasing attention in the past 10 years because visible luminescence was discovered in porous silicon,[1] and more recently, optical gain was observed in silicon nanocrystals.[2,3] Their optical properties are thus of special interest because of the potential application for making optoelectronic devices. It is widely believed that it is the low dimensionality of silicon nanostructures that makes the indirect band gap of bulk silicon at 1.12 eV[4] into larger direct gaps, facilitating reasonably high visible photoluminescence (PL) from the nanostructures compared with the poor PL from bulk silicon. And as the size of bulk silicon decreases beyond the limit of its free-exciton Bohr radius (∼43 Å),[5] the quantum confinement effect would significantly alter the optical behavior of the system, resulting in possible excitations in the visible range.

Many experimental[6−13] and theoretical[14−27] studies have been carried out on the optical properties of hydrogenated silicon clusters, and more are expected to appear because of the controversies over the different methodologies used in experiments and the levels of calculation employed. In fact, both the experimentally and theoretically determined optical properties of hydrogenated silicon clusters are still diverse. In particular, the inconsistent results mainly arise from determining the relationship between the optical gap and the cluster size, though blue shifts were revealed with decreasing size in general. Wilcoxon et al.[8] examined several major PL experimental studies carried out in recent years. The diversity in results was attributed to two main reasons: the uncertainties of the measured cluster size and the purity of the hydrogenated silicon cluster. The latter case involves an oxidized hydrogenated silicon cluster, which would give very different results to the pure one. This experimental study was later supported by a theoretical study carried out by Garoufalis et al.,[15] who employed the time-dependent density functional theory (TDDFT)[28] and the multireference second-order perturbation theory (MR-MP2).[29] The method they adopted in TDDFT was the hybrid nonlocal exchange-correlation functional of Becke, and Lee, Yang, and Parr (B3LYP).[30] They concluded that their calculated results were in excellent agreement with the experimental data on oxygen-free samples. The related issues were also explored in more recent studies on the emission properties of silicon clusters.[31−34] Similar trends of dimensionality-dependent energy gaps were also observed in the absorption spectra of hydrogenated silicon clusters in experiments.[6,7,10]

Although all theoretical studies generally agree that, due to the quantum confinement effect, the optical gap blue shifts as the cluster size decreases, there are obvious deviations in the magnitude of the calculated optical gap so that the inverse relationship between the optical gap and the cluster size is different. This can be attributed to the different approximations for spectrum calculations, including the treatment of Coulomb or excitonic interactions, the screening effects due to the models employed such as the supercell and real-space models, or the adopted boundary conditions. For instance, a recent article compared the time-dependent local density approximation method (TDLDA) and bethe-salpeter equation (BSE) calculations on hydrogenated silicon clusters up to a size of 35 silicon atoms.[17] It was concluded that the exchange-correlation kernel in TDLDA had almost no effect on the calculated spectra, while the corresponding attractive part of the electron−hole interaction in the BSE produced enhanced absorptive features at low energies. Besides, it was pointed out in ref 15 that the different results obtained from the TDDFT/B3LYP and the pseudopotential calculation[16] were perhaps due to the improper treatment in the screening of the exact exchange interaction in the latter calculation.

Thus far, the theoretical methods adopted to calculate the excited-state properties, such as absorption spectra and the relationship between the optical gap and the size, are numerous and include the TDLDA method of Vasiliev et al.,[20] the real-space pseudopotential method of Ö''üt et al.,[21] the BSE approach of Rohlfing et al.,[22] the configuration interaction (CI) method incorporating intermediate neglect of differential overlap (INDO) of Baierle et al.,[19] the independent-particle approximation and the pseudopotential-plane-wave method of Weissker et al.,[18] the TB supercell calculation with use of empirical pseudopotentials of Reboredo et al.,[16] the above-mentioned TDDFT/B3LYP and

10.1021/jp063895w CCC: $33.50
Published on Web 10/04/2006

MR-MP2 methods of Garoufalis et al., and so on. When compared with experimental data, the TDLDA[20] results fit well with experiments reported in refs 6, 7, and 14, while for the BSE,[22] TDDFT/B3LYP,[15] the tight-binding (TB) supercell,[16] and the real-space pseudopotential calculations,[21] the results fit well with experiments reported in refs 6, 8, 9, and 7, respectively. For the ab initio calculations, the largest diameter of the cluster is limited to below ~2 nm. In the studies with the BSE, MR-MP2, CI, TDLDA, LDA, and TDDFT/B3LYP methods, the largest cluster contained respectively 14, 29, 71, 147, 147, and 281 silicon atoms. However, due to the computational limits, the clusters with more than 87 silicon atoms were calculated with the chosen energy thresholds in the study by using the TDLDA and LDA methods, while for the TDDFT/B3LYP calculation, the optical gap of the largest cluster (281 silicon atoms) was approximated from the ground-state DFT calculation. Nevertheless, the system in the TDDFT/B3LYP study remains to date the largest ever handled by an ab initio calculation for a single particle of a hydrogenated silicon cluster. The small sizes of the hydrogenated silicon nanostructures in these calculations therefore limit the explorations of physical quantities that are more relevant to experimental measurements such as the dimensionality dependences of these optical properties including the exciton size.

Though spherical silicon clusters have been intensively studied, the other types of low-dimensional silicon nanostructures such as silicon chain and silicon plane have rarely been explored. The thinnest silicon chain is polysilane while a bundle of such chains can form the so-called silicon nanowires (SiNWs),[35−38] which have recently been fabricated with diameters as small as ~1 nm and lengths of a few tens of micrometers.[39] SiNWs have demonstrated many potential applications regarding their excited-state properties in various fields such as optoelectronic and device fabrication. It is thus interesting to examine the optical properties of the silicon chain as well. Polysilane is a σ-conjugated material and exhibits different backbone conformations. This study focuses on the trans-planar one, which is analogous to silicon clusters in the ⟨110⟩ direction. On the other hand, the optical properties of hydrogenated silicon planes have not been well studied because their detailed structure has not been examined clearly in experiments. A chair-type hexagonal silicon plane is thus assumed in this study, which can act as a bridge between the silicon chain and the silicon cluster. Experimentally, many 1D chainlike polysilanes have been synthesized and their linear and nonlinear spectra measured.[40,41] However, only a few theoretical studies dealing with their optical properties have been carried out. For instance, the electronic structures of Si-skeleton chainlike and planar materials were calculated by the first-principles local-density-functional method, in which the calculated band gap for the former was about 4 eV while the latter had an indirect band gap of 2.48 eV and a direct band gap of 2.68 eV.[42]

In this paper, the absorption spectra and the relationship between the optical gap and the size of hydrogenated silicon chains, silicon planes, and silicon spheres are determined systematically, using the time-dependent Hartree−Fock (TDHF)[43−45] approach incorporating the semiempirical INDO/S Hamiltonian,[46−48] which includes all single electron excitations and partial double, triple, and other multiple electron excitations. It has been applied successfully to simulate optical spectra of many electronic systems such as PPV,[49] carbon nanotubes,[50] and boron−nitride nanotubes.[51] The calculated results are compared with other theoretical data as well as available experimental results. In addition, the real-space density matrices for the first excited state of selected silicon nanostructures are calculated and the exciton sizes are evaluated. We aim to determine the dependence of the exciton size on the dimensionality of silicon nanostructures to examine the quantum confinement effect in more detail.

Computational Methods

The geometries of hydrogenated silicon spherical clusters were determined by using a tight-binding potential model developed by Tagami et al.,[52] which has been applied successfully by us in the study of the structures of hydrogenated silicon nanocrystals and nanoclusters.[53] Since this model is reliable for describing the diamond structure of silicon but not for linear and planar structures, we adopted the crystal geometrical data (2.35 and 1.48 Å for Si−Si and Si−H bond distances, respectively) to construct the geometries of silicon chains and planes.

The INDO/S Hamiltonian used for excited-state calculations in the presence of an external field **E** reads

$$\hat{H} = \sum_{ab}\sum_{i\in a,j\in b} t_{ij}\, c_{ai}^{\dagger}c_{bj} + \frac{1}{2}\sum_{a}\sum_{ijmn} V_a^{ij,mn} c_{ai}^{\dagger}c_{am}^{\dagger}c_{an}c_{aj} + \frac{1}{2}\sum_{a\neq b}\sum_{i\in a,j\in b} \gamma_{ab}^{ij} c_{ai}^{\dagger}c_{ai}c_{bj}^{\dagger}c_{bj} - \mathbf{E}\cdot\sum_{mn}\mathbf{P}_{ab}^{mn} c_{am}^{\dagger}c_{bn} \quad (1)$$

where $c_{ai}^{\dagger}$ (c_{bj}) is the creation (annihilation) operator for an electron at a localized atomic spin spatial orbital i (j) on atom a (b), $V_a^{ij,mn}$ is the center repulsion, and γ_{ab}^{ij} stands for the two-center repulsion.

The one-electron hopping integral t_{ij} may be expressed as

$$t_{ij} = \left\langle \chi_a^i \middle| -\frac{1}{2}\nabla_{\mathbf{r}}^2 + U(\mathbf{r}) \middle| \chi_b^j \right\rangle \quad (2)$$

where χ_i (χ_j) is the ith (jth) atomic orbital on atom a (b), and U(r) is the one-electron potential. The second and the third terms in eq 1 represent the effective electron−electron Columbic interaction. The last term describes the interaction between the valence electrons and an external electric field $\mathbf{E}(t)$, and $\hat{\mathbf{P}}$ is the molecular dipole moment operator. $\mathbf{P}_{ab}^{ij}$ is calculated by $\langle\chi_a^i|\hat{\mathbf{P}}|\chi_b^j\rangle$, neglecting the diatomic overlap. Taking into account the linear response only, ρ may be written as $\rho = \rho^{(0)} + \delta\rho$, where $\rho^{(0)}$ is the ground-state reduced density matrix, and $\delta\rho$ is the field-induced density matrix deviation. Similarly, the Fock matrix h can be decomposed into $h = h^{(0)} + \delta h$, where $h^{(0)}$ is the Fock matrix in the absence of the external field:

$$h_{ab}^{(0)mn} = t_{ab}^{mn} + \delta_{ab}\left[2\sum_{ij\in a}\left(V_a^{mn,ij}\,\rho_{aa}^{(0)ij} - \frac{1}{2}V_a^{mi,nj}\,\rho_{aa}^{(0)ij}\right)\right] + \delta_{ab}\delta_{mn}\sum_{c\neq a}\sum_{l\in c} 2\rho_{cc}^{ll}\,\gamma_{ac}^{ml} - \rho_{ba}^{(0)nm}\,\gamma_{ab}^{mn} \quad (3)$$

and similarly, the field-induced Fock matrix can be written as

$$\delta h_{ab}^{mn} = \delta_{ab}\left[2\sum_{ij\in a}\left(V_a^{mn,ij}\,\delta\rho_{aa}^{(0)ij} - \frac{1}{2}V_a^{mi,nj}\,\delta\rho_{aa}^{(0)ij}\right)\right] + \delta_{ab}\delta_{mn}\sum_{c\neq a}\sum_{l\in c} 2\delta\rho_{cc}^{ll}\,\gamma_{ac}^{ml} - \delta\rho_{ba}^{nm}\,\gamma_{ab}^{mn} \quad (4)$$

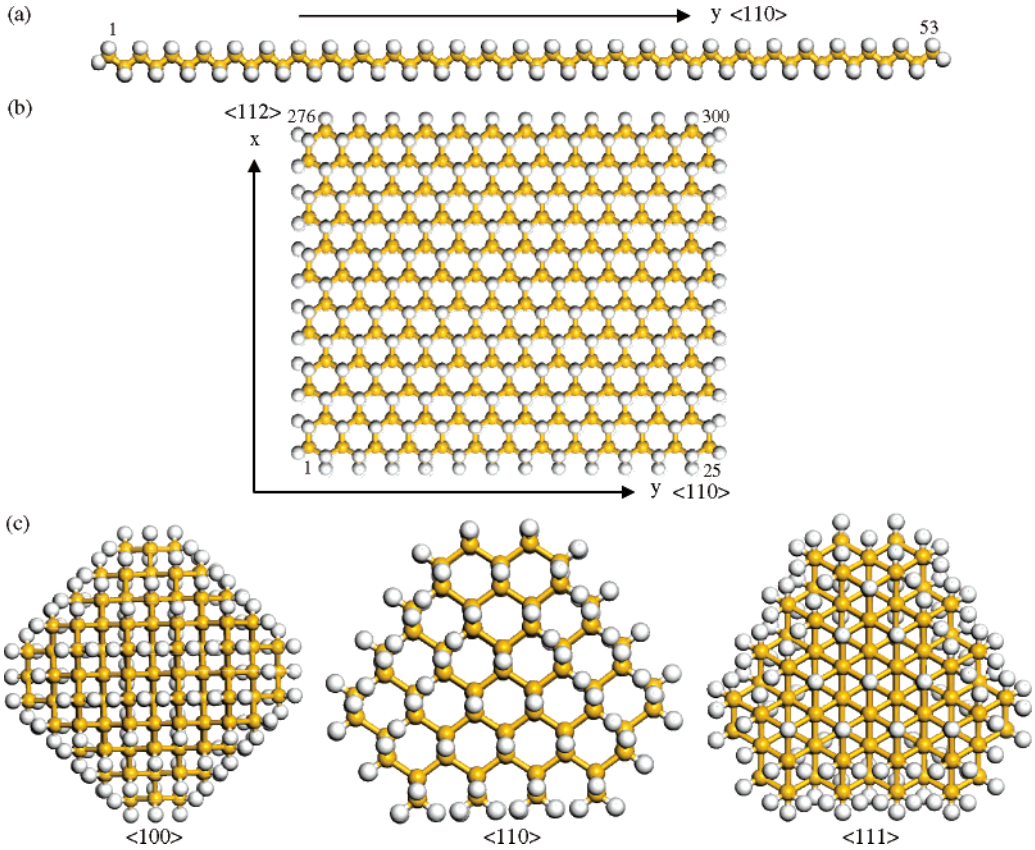

Figure 1. The structures of (a) silicon chain ($Si_{53}H_{108}$), (b) silicon plane ($Si_{300}H_{348}$), and (c) silicon cluster ($Si_{199}H_{140}$) viewed from ⟨100⟩ , ⟨110⟩, and ⟨111⟩ directions. Silicon and hydrogen atoms are shown as yellow and white balls, respectively. The numbers show the labeling of the silicon chain and the silicon plane. The labeling of the silicon cluster is along the ⟨110⟩ direction. The axes label the spatial coordinates.

The single-electron density matrix follows the equation of motion:

$$\left(i\hbar\frac{\mathrm{d}}{\mathrm{d}t}+\gamma\right)\delta\rho(t)=[h^{(0)},\delta\rho(t)]+[\delta h(t),\rho^{(0)}]-\mathbf{E}(t)\cdot[\mathbf{P},\rho^{(0)}] \quad (5)$$

Equation 5 is then solved in the time domain for the time evolution of the polarization vector $\mathbf{P}(t)$. Within the dipole approximation, $\mathbf{P}(t)$ may be expressed as

$$\mathbf{P}(t)=\sum -e\langle\chi_i|\hat{r}|\chi_j\rangle\rho_{ij}(t) \quad (6)$$

To obtain the optical absorption spectrum, a Fourier transformation of $\mathbf{P}(t)$ is performed:

$$\mathbf{P}(\omega)=\int_{-\infty}^{\infty}\partial t\,\mathbf{P}(t)\,e^{-i\omega_t} \quad (7)$$

The imaginary part $\alpha(\omega)$ of the complex linear polarizability, which represents the absorption spectrum, is then determined readily via

$$\alpha(\omega)=\mathrm{Im}[\mathbf{P}(\omega)/\epsilon(\omega)] \quad (8)$$

where $\epsilon(\omega)$ is the Fourier transform of $\epsilon(t)$.

The INDO/S parametrization is mainly based on the original work of Ridley et al.[48] and Bacon et al.[54] Only the bonding parameter (β) of silicon is different: −9.4 eV is employed in this study. This gives the best fit of the experimental lowest dipole-allowed absorption energy (6.5 eV)[14] for a spherical Si_5H_{12} cluster. Similar β values, −9.0 and −9.5 eV, were employed respectively in refs 55 and 56, where the absorption spectra of molecules containing silicon atoms were calculated by the configuration interaction (CI) method. The accuracy of the INDO/S parametrization is achieved by matching it with the experimental absorption data of various small molecules. The resulting parametrization can then be applied to large molecules directly. This gives the advantage over some tight-binding semiempirical schemes that uncertainties resulting from the transferability of using bulk material parameters in nanosized material calculations are avoided.

Results and Discussion

The Structures. We examine a series of silicon chains (Si_3H_8, Si_5H_{12}, Si_7H_{16}, Si_9H_{20}, $Si_{39}H_{80}$, and $Si_{53}H_{108}$), silicon planes ($Si_{25}H_{52}$, $Si_{50}H_{78}$, $Si_{100}H_{132}$, $Si_{150}H_{186}$, $Si_{200}H_{240}$, and $Si_{300}H_{348}$), and silicon spherical clusters (Si_5H_{12}, $Si_{17}H_{36}$, $Si_{29}H_{36}$, $Si_{41}H_{60}$, $Si_{59}H_{60}$, $Si_{83}H_{108}$, $Si_{123}H_{100}$, and $Si_{199}H_{140}$). The surfaces of all silicon nanostructures are fully terminated by hydrogen atoms in order to saturate the dangling bonds, which can strongly affect the absorption spectrum. The silicon chain is of trans-planar geometry while a chair-type hexagonal Si-skeleton network structure is adopted for the silicon plane. The structures of the silicon chain ($Si_{53}H_{108}$), the silicon plane ($Si_{300}H_{348}$), and the silicon cluster ($Si_{199}H_{140}$) are shown respectively in parts a−c of Figure 1. In this study, the longest chain is ∼10.0 nm in length while the largest cluster is ∼1.9 nm in diameter. The largest plane has a length of ∼4.6 nm and a width of ∼3.7 nm. The measured sizes exclude hydrogen atoms. The optimized silicon clusters have an average Si−Si distance of 2.35 to 2.36 Å in the inner shells and 2.34 Å in the outer shells. A small surface contraction is observed. The Si−H distance is about 1.48 Å on average. The optimized Si−Si distance agrees perfectly with the experimental value 2.352 Å[31] of crystal silicon. All bonds in the silicon nanostructures are tetrahedral.

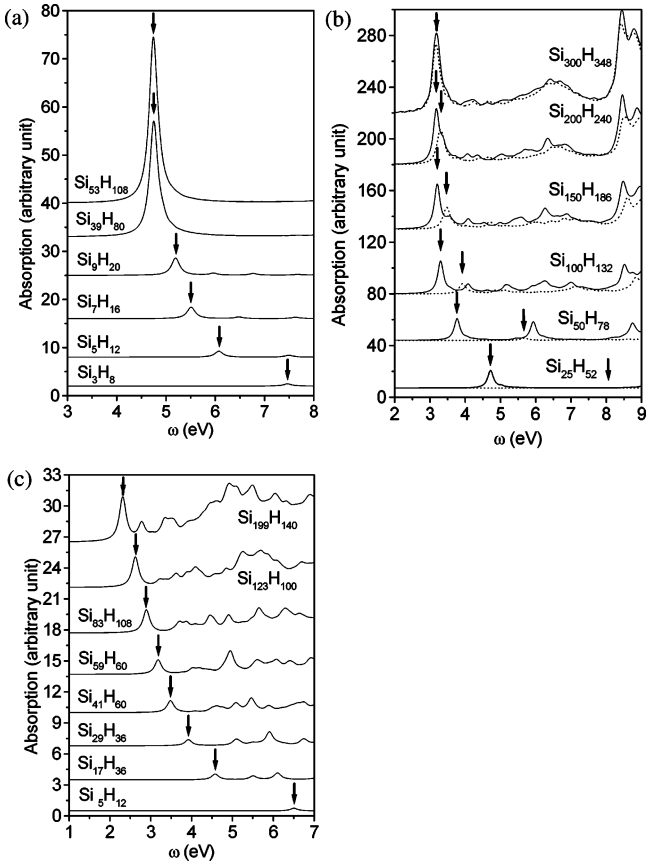

Figure 2. The absorption spectra for (a) silicon chains, (b) silicon planes, and (c) silicon clusters. The arrow indicates the lowest absorption peak for each cluster. The dephasing parameter (γ) for each absorption spectrum is 0.1 eV.

TABLE 1: Calculated Optical Gaps and Absorption Intensities for Silicon Chains

		E field applied along the *y* direction	
silicon chain	length (nm)	optical gap (eV)	abs intensity (arb. unit)
Si_3H_8	0.36	7.46	0.45
Si_5H_{12}	0.77	6.07	1.24
Si_7H_{16}	1.15	5.51	2.39
Si_9H_{20}	1.54	5.19	3.61
$Si_{39}H_{80}$	7.29	4.77	24.10
$Si_{53}H_{108}$	9.98	4.74	34.54

Optical Spectra. The absorption spectra of all silicon nanostructures are shown in Figure 2. The arrow indicates the lowest peak position for each spectrum. The absorption is in an arbitrary unit but the relative peak heights are comparable. The absorption spectra of six silicon chains (Si_3H_8, Si_5H_{12}, Si_7H_{16}, Si_9H_{20}, $Si_{39}H_{80}$, and $Si_{53}H_{108}$) are shown in Figure 2a, in which the lengths ranged from 0.36 to 9.98 nm. The electric field is applied along the chain direction. It is observed that only one major absorption peak appears below 8 eV in each spectrum. This characteristic peak arises from the σ-conjugation of the silicon chain. The peak tends to saturate at around 4.7 eV when the length of the chain is ~2.5 nm. The saturation has to be achieved to avoid the constraint of exciton due to the physical size. The optical data for all silicon chains are summarized in Table 1.

The absorption spectra of six silicon planes ($Si_{25}H_{52}$, $Si_{50}H_{78}$, $Si_{100}H_{132}$, $Si_{150}H_{186}$, $Si_{200}H_{240}$, and $Si_{300}H_{348}$) are shown in Figure 2b. The length of each plane is fixed at 4.58 nm while the widths vary from 0.12 to 3.74 nm. The length lies along the *y* direction while the width lies along the *x* direction (see Figure 1b). The chosen length should already be large enough to avoid the physical constraint of exciton in the *y* direction, as in the case of the silicon chain. The solid lines in Figure 2b represent the absorption spectra when the electric field is applied in the *y* direction while the dotted lines represent the absorption spectra when the electric field is applied in the *x* direction (see Figure 1b). For the plane with the thinnest width ($Si_{25}H_{52}$), the lowest absorption peak arising from the *x* direction is ~8.0 eV while in the *y* direction, it is ~4.7 eV. Moreover, the absorption intensity is very small in the former case while the latter case is ~170 times larger. This observation is due to the strong anisotropic effects, which reflect its one-dimensional nature. However, as the width increases, the lowest peaks in both the *x* and *y* directions red shift and become close to each other. Simultaneously, the absorption intensity increases readily for the lowest peak in the *x* direction as the width increases. The two spectra should merge into each other as the size of the plane is large enough in both dimensions. This shows that the silicon plane has the doubly degenerate first excited state. In addition, the lowest peak starts to saturate at a size of ~2.5 nm, which is very similar to the case of the silicon chain. The optical data for the silicon planes are summarized in Table 2.

TABLE 2: Calculated Optical Gaps and Absorption Intensities for Silicon Planes[a]

		E field applied along the *y* direction		*E* field applied along the *x* direction	
silicon plane	width (nm)	optical gap (eV)	abs intensity (arb. unit)	optical gap (eV)	abs intensity (arb. unit)
$Si_{25}H_{52}$	0.12	4.78	13.67	8.06	0.08
$Si_{50}H_{78}$	0.45	3.77	16.79	5.68	1.80
$Si_{100}H_{132}$	1.10	3.30	25.42	3.92	7.89
$Si_{150}H_{186}$	1.76	3.21	34.92	3.48	16.87
$Si_{200}H_{240}$	2.42	3.19	43.40	3.31	27.07
$Si_{300}H_{348}$	3.74	3.18	61.79	3.18	53.41

[a] Length for each plane is 4.58 nm.

The absorption spectra of eight silicon spherical clusters (Si_5H_{12}, $Si_{17}H_{36}$, $Si_{29}H_{36}$, $Si_{41}H_{60}$, $Si_{59}H_{60}$, $Si_{83}H_{108}$, $Si_{123}H_{100}$, and $Si_{199}H_{140}$) are shown in Figure 2c. The diameters range from 0.38 to 1.92 nm. The absorption spectra when the electric field is applied in the ⟨110⟩ direction are presented. The absorption spectrum of Si_5H_{12} shows a unique peak at ~6.5 eV while the absorption spectrum of $Si_{199}H_{140}$ shows multiple peaks. This is evidence that as the size of the cluster decreases, the direct gap nature becomes more significant, similar to cases of the silicon chain. In addition, the lowest peak tends not to saturate at a diameter up to ~1.9 nm, implying that the exciton in these clusters should still be confined. It is also the case that the characteristic of the absorption spectrum of the silicon plane, with regard to both the absorption gap and intensity, is intermediate between the silicon chain and the silicon spherical cluster. The optical data for silicon spherical clusters are summarized in Table 3, in which the calculated optical gaps for the silicon clusters are basically the same no matter whether the excitation is induced from the ⟨110⟩ , ⟨111⟩ , or ⟨100⟩ direction. This reflects the spherical nature of the cluster so that it has the triply degenerate first excited state.

The plots of optical gaps as a function of chain lengths, plane widths, and cluster diameters are shown respectively in parts a−c of Figure 3. The extrapolated optical gaps at the infinite size for the silicon chain, the silicon plane, and the silicon spherical cluster are ~4.7, ~3.1, and ~2.0 eV, respectively. For the silicon chain, the result agrees very well with the first-principles pseudopotential calculation of a polysilane molecule,

TABLE 3: Calculated Optical Gaps and Absorption Intensities for Silicon Clusters

		E field applied along the ⟨110⟩ direction		*E* field applied along the ⟨111⟩ direction		*E* field applied along the ⟨100⟩ direction	
silicon cluster	diameter (nm)	optical gap (eV)	abs intensity (arb. unit)	optical gap (eV)	abs intensity (arb. unit)	optical gap (eV)	abs intensity (arb. unit)
Si_5H_{12}	0.38	6.51	0.25	6.51	0.25	6.51	0.25
$Si_{17}H_{36}$	0.77	4.58	0.57	4.57	0.56	4.58	0.57
$Si_{29}H_{36}$	0.76	3.92	0.59	3.92	0.60	3.92	0.59
$Si_{41}H_{60}$	1.16	3.48	1.16	3.48	1.17	3.48	1.17
$Si_{59}H_{60}$	1.15	3.18	1.42	3.19	1.42	3.18	1.42
$Si_{83}H_{108}$	1.55	2.89	2.25	2.89	2.23	2.89	2.23
$Si_{123}H_{100}$	1.53	2.62	2.98	2.62	2.97	2.62	2.96
$Si_{199}H_{140}$	1.92	2.32	4.41	2.32	4.41	2.32	4.41

TABLE 4: Comparison of the Optical Gaps of Spherical Cluster $Si_{29}H_{36}$ from Different Sources

	theoretical method					expt
	TDDFT B3LYP[15]	TDLDA[20]	CI[19]	TDDFT BP/TZVP[27]	our approach	refs 27 and 58
optical gap (eV) of $Si_{29}H_{36}$	4.53	~4.5	~3.4	3.85	3.92	3.7

which yielded a direct band gap of 4.69 eV.[57] So far, there are no experimental optical data for any silicon plane. However, the optical gap of ~3.1 eV is reasonable as it falls between the optical gaps of the silicon chain and the silicon cluster. In ref 42, the calculated band gap for the silicon chain was about 4 eV while the direct band gap of planar silicon was 2.68 eV. The first-principles local-density-functional method was applied in this earlier study. Our results are larger but still consistent with these earlier results. The deviation may be attributed to the different levels of theory employed. For the silicon spherical cluster, the trend matches excellently with the general observation for quantum-confined silicon clusters that the optical gap increases as the cluster size decreases. For spherical clusters $Si_{17}H_{36}$ and $Si_{29}H_{36}$, $Si_{41}H_{60}$ and $Si_{59}H_{60}$, and $Si_{83}H_{108}$ and $Si_{123}H_{100}$, each pair has a similar diameter. The difference in the optical gap arises from the total number of silicon atoms that the cluster possesses. The one with a lower optical gap contains facets in its structure. It is interesting to note that the influence of a facet decreases as the cluster size increases. So, these two curves are expected to coincide at a larger cluster size. The plot of the optical gaps as a function of silicon atoms is shown for comparison. Furthermore, to compare our results with other theoretical calculations such as TDDFT, TDLDA, and CI, the spherical cluster $Si_{29}H_{36}$ is taken as an example. The comparison is summarized in Table 4. The result reveals that our calculation is fairly accurate. The extrapolation of the optical gap is expected to saturate at ~2 eV when the diameter of the silicon spherical cluster increases infinitely.

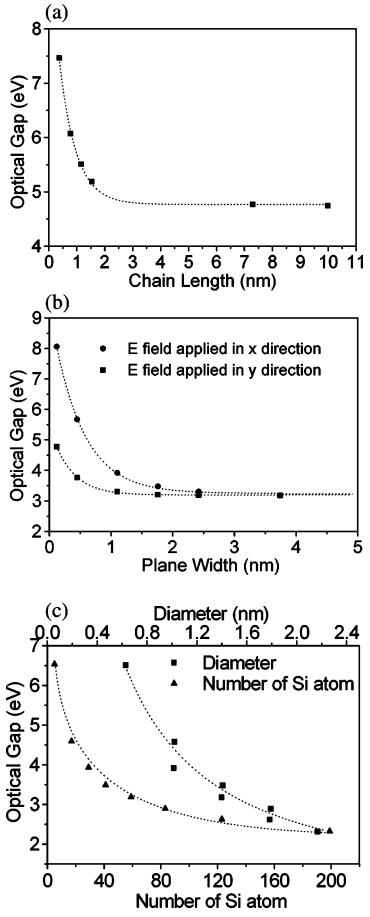

Figure 3. Variation of optical gaps as a function of sizes for (a) silicon chain, (b) silicon plane, and (c) silicon cluster. In panel b, the electric field is applied along the *x* direction (circle) and the *y* direction (square), see Figure 1b. In panel c, optical gaps as functions of diameter (square) and the number of silicon atoms (triangle) are plotted for comparison. The dotted lines are guides for the eyes.

Density Matrices and the Excitons. To evaluate how the exciton size is related to the shape of silicon structures, the contour plots of the first excited-state density matrix of selected silicon nanostructures are examined. The density matrix element $c_{i,j}$ between atom i and atom j is evaluated by

$$c_{i,j} = (1 - \delta_{ij})\sqrt{\sum_{\nu_1\nu_2} |\delta\rho_{ij}^{\nu_1\nu_2}(\omega)|^2} \qquad (9)$$

where $\delta\rho_{ij}^{\nu_1\nu_2}(\omega)$ is obtained by the Fourier transformation of $\delta\rho_{ij}^{\nu_1\nu_2}(t)$. This represents the off-diagonal density matrix between two atoms, averaged over various orbitals ν. The first excited-state density matrices for silicon chains Si_9H_{20}, $Si_{39}H_{80}$, and $Si_{53}H_{108}$ are shown respectively in parts a−c of Figure 4. The off-diagonal part of the contour plot represents the electronic coherences induced by the electric field at a given frequency ω. The darkness of the contour represents the distribution of the matrix elements. The darker the corresponding contour line, the larger are the electronic coherences. The real-space density matrix analysis allows a direct interpretation of the optical excitation. Since silicon chains are purely one-dimensional, the axes of the density matrix label the silicon atoms along the *y* direction (see Figure 1a). For instance, Figure 4a is a 9-by-9 matrix because Si_9H_{20} contains nine silicon atoms. From the three density matrices, it is obvious that the extent of electronic

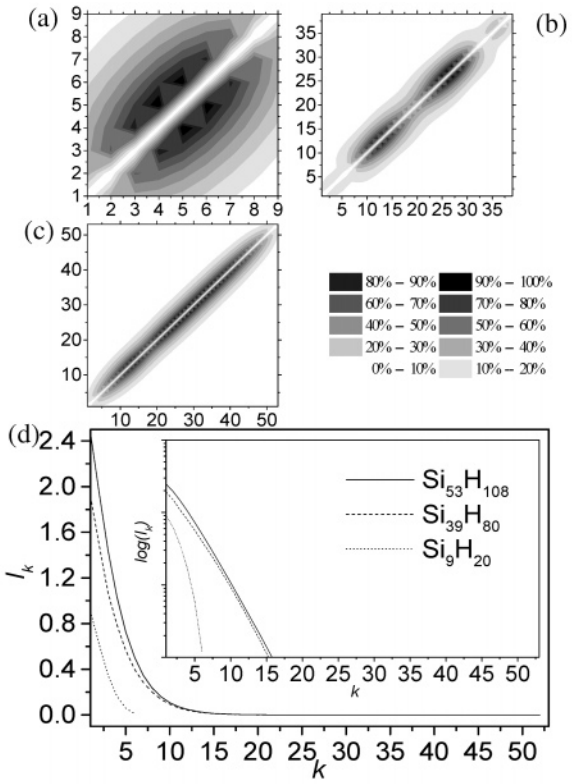

Figure 4. The first excited-state density matrices for silicon chains (a) Si_9H_{20}, (b) $Si_{39}H_{80}$, and (c) $Si_{53}H_{108}$. The legend is the scale for the density matrices. (d) Plots of I_k vs atom index k for Si_9H_{20} (dotted line), $Si_{39}H_{80}$ (dashed line), and $Si_{53}H_{108}$ (solid line). The inset shows I_k in log scale.

coherences is confined by the physical size of Si_9H_{20}; that is, the wide spread of matrix elements in the whole plot, in contrast to the diagonal-like density matrices for $Si_{39}H_{80}$ and $Si_{53}H_{108}$ (Figure 4, parts b and c), in which the physical size of the chain is very large. The exciton size can be determined by summing the density matrix elements along the direction of the diagonal of the plot as follows:

$$\sum_{n=1}|\delta\rho_{n,n}| = I_1$$

$$\sum_{n=1}|\delta\rho_{n,n+1}| = I_2$$

$$\vdots$$

$$\sum_{n=1}|\delta\rho_{n,n+(k-1)}| = I_k$$

$$\vdots$$

$$\sum_{n=1}|\delta\rho_{n,n+(N-1)}| = I_N$$

where $\delta\rho$ is the density matrix element, n is the specified atom, and N is the total number of atoms. The plots of I_k versus the atom index k for Si_9H_{20}, $Si_{39}H_{80}$, and $Si_{53}H_{108}$ are shown in Figure 4d. The inset shows I_k in log scale. The width of the density matrix is approximated by the value of the index k_0, where $I_{k0} = 0$. k_0 is thus found to be ~15 for $Si_{39}H_{80}$ and $Si_{53}H_{108}$. The corresponding exciton size is ~26 Å for these two silicon chains, which is equivalent to a spread over 15 silicon atoms. For Si_9H_{20}, it is obvious that no convergence is

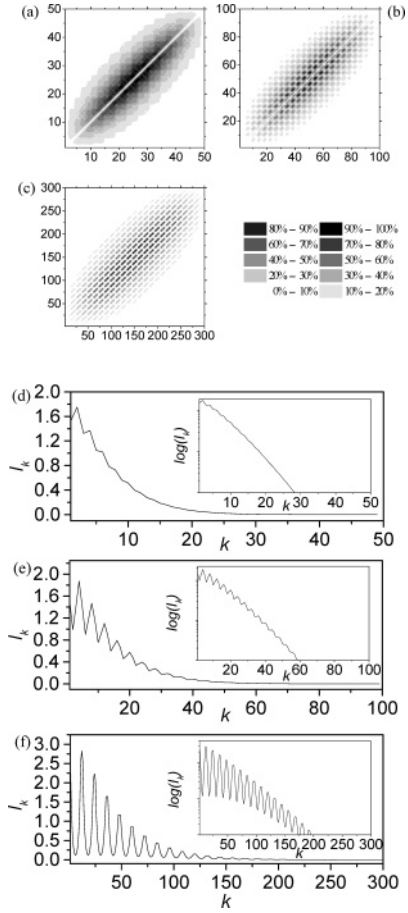

Figure 5. The first excited-state density matrices for silicon planes (a) $Si_{50}H_{78}$, (b) $Si_{100}H_{132}$, and (c) $Si_{300}H_{348}$. The legend is the scale for the density matrices. Plots of I_k vs atom index k for (d) $Si_{50}H_{78}$, (e) $Si_{100}H_{132}$, and (f) $Si_{300}H_{348}$. The insets show I_k in log scale.

observed in both plots, implying that the physical size of this chain is not large enough to determine the exciton size of the system.

A similar analysis is conducted for the silicon planes. The first excited-state density matrices for silicon planes $Si_{50}H_{78}$, $Si_{100}H_{132}$, and $Si_{300}H_{348}$ are shown respectively in parts a−c of Figure 5. The axes of the density matrix label the silicon atoms in the y direction (see Figure 1b). The length of the plane is kept at 4.58 nm, and this value is much larger than the exciton size in the silicon chain, the aim here being to examine how the exciton size changes with the width. The plots of I_k versus the atom index k for $Si_{50}H_{78}$, $Si_{100}H_{132}$, and $Si_{300}H_{348}$ are shown respectively in parts d−f of Figure 5. The inset shows I_k in log scale. The width of the density matrix is approximated by the value of the index k_0, where $I_{k0} = 0$. k_0 is thus found to be ~29 for $Si_{50}H_{78}$, ~60 for $Si_{100}H_{132}$, and ~184 for $Si_{300}H_{348}$. An exciton size of ~26 Å is found for the three planes. It is thus revealed that the exciton size does not change at all as the width increases. As silicon planes have a doubly degenerate state, the exciton size measured in the x direction should also be ~26 Å. Since the size for $Si_{300}H_{348}$ should be large enough to avoid the physical constraint of exciton, we conclude here that the exciton size determined from the silicon planes is basically the same as that determined from the silicon chains.

Finally, the density matrices of silicon spherical clusters $Si_{17}H_{36}$, $Si_{59}H_{60}$, $Si_{123}H_{100}$, and $Si_{199}H_{140}$ are examined. Since the density matrix of the whole three-dimensional cluster is very complicated due to its spherical shape, the density matrices shown in Figure 6 are simplified by plotting a set of silicon

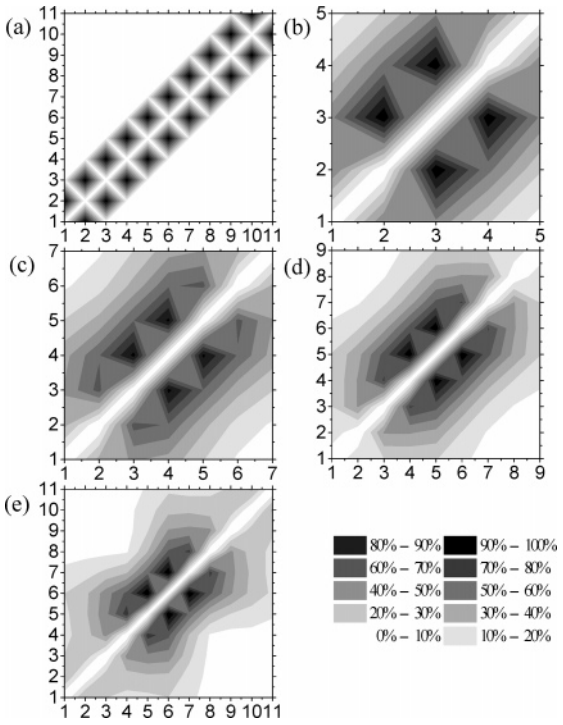

Figure 6. (a) The ground-state density matrix for $Si_{199}H_{140}$. The first excited-state density matrices for clusters (b) $Si_{17}H_{36}$, (c) $Si_{59}H_{60}$, (d) $Si_{123}H_{100}$, and (e) $Si_{199}H_{140}$. The legend is the scale for the density matrices.

atoms along the ⟨110⟩ direction passing through the central atom of the cluster. The numbers of atoms along the ⟨110⟩ direction are 5, 7, 9, and 11 for $Si_{17}H_{36}$, $Si_{59}H_{60}$, $Si_{123}H_{100}$, and $Si_{199}H_{140}$, respectively. The axes of the density matrix label the silicon atoms along the ⟨110⟩ direction. So, labels 3, 4, 5, and 6 are the central atoms for $Si_{17}H_{36}$, $Si_{59}H_{60}$, $Si_{123}H_{100}$, and $Si_{199}H_{140}$, respectively. The ground-state density matrix of $Si_{199}H_{140}$ is shown in Figure 6a. The ground-state density matrix is obtained by replacing $\delta\rho$ with $\rho^{(0)}$ in eq 9. The ground state correlation is of very short range: only electrons on the nearest neighbor and the next-nearest neighbor are correlated. This is the case for all other silicon nanostructures. The ground-state coherent size is about 7.7 Å for the silicon cluster. However, the electronic coherences are of much greater extent in the excited state. The first excited-state density matrices for $Si_{17}H_{36}$, $Si_{59}H_{60}$, $Si_{123}H_{100}$, and $Si_{199}H_{140}$ are shown respectively in parts b−e of Figure 6. It is obvious that the extent of electronic coherences is spread over the whole cluster. Moreover, all excited state density matrices show clearly that the matrix elements have their largest value around the central atom of each cluster. It is thus concluded that the exciton of the lowest excited state is mainly concentrated near the cluster center. A similar conclusion was obtained for CdSe nanocrystal in ref 59. As reflected by the density matrices, it is confirmed here that a silicon spherical cluster with a diameter of ∼1.9 nm is still quantum confined.

Further Comparison. It has been shown that the optical properties of silicon nanostructures with different shapes are remarkably different. Further comparisons can be made for silicon chains and silicon spherical clusters in terms of (i) a similar number of silicon atoms and (ii) a similar length/diameter. For (i), the silicon chain $Si_{39}H_{80}$ and the silicon cluster $Si_{41}H_{60}$ are compared. The silicon chain possesses a larger optical gap as well as a larger absorption intensity. The absorption intensity for this chain is about seven times greater than that of this cluster, which is consistent with the change of the gap nature from a direct gap to an indirect gap. For (ii), the silicon chain Si_9H_{20} and the silicon cluster $Si_{123}H_{100}$ are compared. The optical gap of the chain is larger but the absorption intensity for the cluster is about 2.5 times greater. The corresponding density matrices are shown in Figures 4a and 6d, each being a 9-by-9 matrix. The structure of the trans-planar silicon chain and the set of silicon atoms in the ⟨110⟩ direction of the cluster are similar. Both density matrices are generally similar in terms of the overall pattern of the contour. The minor difference can be attributed to the uniform structure of the silicon chain while the spherical cluster exhibits surface contraction. We concluded previously that both the silicon chain and the silicon plane have a similar exciton size of ∼26 Å, which suggests that no significant change of exciton size is observed when the dimension of the nanostructure increases; so we expect that the silicon cluster would possess a similar exciton size. Zhao et al.[60] reported that quantum confinement of silicon nanowires became significant for diameters smaller than 2.2 nm. Read et al.[57] concluded that the effective mass theory (EMT) gave a good description of the electronic states for silicon wires wider than 23 Å, but thinner wires showed significant deviation from the EMT picture. Both studies provided similar values that are comparable to ours for the quantum confinement effect in silicon nanostructures. As a result, we suggest that the quantum confinement effect for hydrogenated silicon nanostructures is crucial when its physical size is smaller than the exciton size but is less dependent on the geometry.

Conclusion

The excited state properties of hydrogenated silicon chains, silicon planes, and silicon clusters, which represent the linear, planar, and spherical geometries, have been studied systematically. The calculated absorption spectra and optical gaps of all silicon nanostructures fall in trends that are generally consistent with other theoretical studies as well as with the available experimental data. Such optical properties are affected not only by size but also by shape, as indicated by the fact that the optical gap depends on the shape of the nanostructures. On the other hand, we have demonstrated the quantum confinement effect as well as the determination of the exciton size via the first excited-state density matrix. The exciton size is calculated to be ∼26 Å for silicon chains and silicon planes, and we expect clusters would have a similar value. The quantum confinement effect should then be significantly enhanced when their size is smaller than ∼26 Å. We suggest that the quantum confinement effect for hydrogenated silicon nanostructures is crucial at a typical physical size but is less dependent on the geometry. The present study should provide some important information to facilitate the designs and applications of nanoscaled-silicon-based materials, such as in the field of optoelectronic devices.

Acknowledgment. The work described in this paper is supported by City University of Hong Kong (Project No. 7001685) and the Research Grants Council of Hong Kong SAR [project Nos. CityU 103305 and CityU 3/04C]. We thank Dr. S. Yokojima, Dr. W. Z. Liang, and Prof. G. H. Chen, the authors of the TDHF program we used in this work.

References and Notes

(1) Canham, L. T. *Appl. Phys. Lett.* **1990**, *57*, 1046.

(2) Pavesi, L.; Negro, L. Dal.; Mazzoleni, C.; Franzò, G.; Priolo, F. *Nature* **2000**, *408*, 440.

(3) Negro, L. Dal.; Cazzanelli, M.; Pavesi, L.; Ossicini, S.; Pacifici, D.; Franzò, G.; Priolo, F. *Appl. Phys. Lett.* **2003**, *82*, 4636.

(4) Cullis, A. G.; Canham, L. T.; Calcott, P. D. J. *J. Appl. Phys*. **1997**, *82*, 909.
(5) Delerue, C.; Allan, G.; Lannoo, M. *Phys. Rev. B* **1993**, *48*, 11024.
(6) Itoh, U.; Toyoshima, Y.; Onuki, H.; Washida, N.; Ibuki, T. *J. Chem. Phys*. **1986**, *85*, 4867.
(7) Furukawa, S.; Miyasato, T. *Phys. Rev. B* **1988**, *38*, 5726.
(8) Wilcoxon, J. P.; Samara, G. A.; Provencio, P. N. *Phys. Rev. B* **1999**, *60*, 2704.
(9) Calcott, P. D. J.; Nash, K. J.; Canham, L. T.; Kane, M. J.; Brumhead, D. *J. Phys.*: *Condens. Matter* **1993**, *5*, L91.
(10) Lockwood, D. J.; Wang, A.; Bryskiewicz, B. *Solid State Commum*. **1994**, *89*, 587.
(11) Wolkin, M. V.; Jorne, J.; Fauchet, P. M.; Allan, G.; Delerue, C. *Phys. Rev. Lett*. **1999**, *82*, 197.
(12) Kim, K. *Phys. Rev. B* **1998**, *57*, 13072.
(13) Kanemitsu, Y. *Phys. Rev. B* **1994**, *49*, 16845.
(14) Delley, B.; Steigmeier, E. F. *Phys. Rev. B* **1993**, *47*, 1397.
(15) Garoufalis, C. S.; Zdetsis, A. D.; Grimme, S. *Phys. Rev. Lett*. **2001**, *87*, 276402.
(16) Reboredo, F. A.; Franceschetti, A.; Zunger, A. *Phys. Rev. B* **2000**, *61*, 13073.
(17) Benedict, L. X.; Puzder, A.; Williamson, A. J.; Grossman, J. C.; Galli, G.; Klepeis, J. E.; Raty, J.-Y.; Pankratov, O. *Phys. Rev. B* **2003**, *68*, 085310.
(18) Weissker, H.-Ch.; Furthmüller, J.; Bechstedt, F. *Phys. Rev. B* **2002**, *65*, 155328.
(19) Baierle, R. J.; Caldas, M. J.; Molinari, E.; Ossicini, S. *Solid State Commun*. **1997**, *102*, 545.
(20) Vasiliev, I.; Ö''üt, S.; Chelikowsky, J. R. *Phys. Rev. Lett*. **2001**, *86*, 1813.
(21) Ö''üt, S.; Chelikowsky, J. R.; Louie, S. G. *Phys. Rev. Lett*. **1997**, *79*, 1770.
(22) Rohlfing, M.; Louie, S. G. *Phys. Rev. Lett*. **1998**, *80*, 3320.
(23) Takagahara, T.; Takeda, K. *Phys. Rev. B*, **1992**, *46*, 15578.
(24) Hill, N. A.; Whaley, K. B. *Phys. Rev. Lett*. **1995**, *75*, 1130. Hill, N. A.; Whaley, K. B. *Phys. Rev. Lett*. **1996**, *76*, 3039.
(25) Delerue, C.; Lannoo, M.; Allan, G. *Phys. Rev. Lett*. **2000**, *84*, 2457.
(26) Wang, L.-W.; Zunger, A. *J. Phys. Chem.* **1994**, *98*, 2158. Wang, L.-W.; Zunger, A. *J. Chem. Phys.* **1994**, *100*, 2394.
(27) Sundholm, D. *Nano Lett*. **2003**, *3*, 847.
(28) Casida, M. E. *Recent Advances in Density Functional Methods*; Chong D. P., Ed.; World Scientific: Singapore, 1995.
(29) Murphy, R. B.; Messmer, R. P. *Chem. Phys. Lett*. **1991**, *183*, 443. Murphy, R. B.; Messmer, R. P. *J. Chem. Phys*. **1992**, *97*, 4170.
(30) Stephens, P. J.; Devlin, F. J.; Chabalowski, C. F.; Frisch, M. J. *J. Phys. Chem*. **1994**, *98*, 11623.
(31) Degoli, E.; Cantele, G.; Luppi, E.; Magri, R.; Ninno, D.; Bisi, O.; Ossicini, S. *Phys. Rev. B* **2004**, *69*, 155411.
(32) Luppi, E.; Degoli, E.; Cantele, G.; Ossicini, S.; Magri, R.; Ninno, D.; Bisi, O.; Pulci, O.; Onida, G.; Gatti, M.; Incze, A.; Sole, R. D. *Opt. Mater*. **2005**, *27*, 1008.
(33) Sundholm, D. *Phys. Chem. Chem. Phys.* **2004**, *6*, 2044.
(34) Puzder, A.; Williamson, A. J.; Grossman, J. C.; Galli, G. *J. Am. Chem. Soc*. **2003**, *125*, 2786.
(35) Morales, A. M.; Lieber, C. M. *Science* **1998**, *279*, 208.
(36) Zhang, Y. F.; Tang, Y. H.; Wang, N.; Yu, D. P.; Lee, C. S.; Bello I.; Lee, S. T. *Appl. Phys. Lett.* **1998**, *72*, 1835.
(37) Holmes, J. D.; Johnston, K. P.; Doty, R. C.; Korgel, B. A. *Science* **2000**, *287*, 1471.
(38) Zhang, R. Q.; Lifshitz, Y.; Lee, S. T. *Adv. Mater*. **2003**, *15*, 639 and references therein.
(39) Ma, D. D. D.; Lee, C. S.; Au, F. C. K.; Tong, S. Y.; Lee, S. T. *Science* **2003**, *299*, 1874.
(40) Tachibana, H.; Matsumoto, M.; Tokura, Y.; Moritomo, Y.; Yamaguchi, A.; Koshihara, S.; Miller, R. D.; Abe, S. *Phys. Rev. B* **1993**, *47*, 4363.
(41) Hasegawa, T.; Iwasa, Y.; Koda, T.; Kishida, H.; Tokura, Y.; Wada, S.; Tashiro, H.; Tachibana, H.; Matsumoto, M. *Phys. Rev. B* **1996**, *54*, 11365.
(42) Takeda, K.; Shiraishi, K. *Phys. Rev. B* **1989**, *39*, 11028.
(43) Takahashi, A.; Mukamel, S. *J. Chem. Phys.* **1994**, *100*, 2366.
(44) Ring, P.; Schuck, P. *The Nuclear Many-Body Problem*; Springer: New York, 1980.
(45) Wagersreiter, T.; Mukamel, S. *Chem. Phys.* **1996**, *210*, 171.
(46) Pople, J. A.; Segal, G. A. *J. Chem. Phys*. **1965**, *43*, S136.
(47) Pople, J. A.; Beveridge, D. L.; Dobosh, P. A. *J. Chem. Phys*. **1967**, *47*, 2026.
(48) Ridley, J.; Zerner, M. *Theor. Chim. Acta* **1973**, *32*, 111.
(49) Ng, M.-F.; Sun, S. L.; Zhang, R. Q. *J. Appl. Phys.* **2005**, *97*, 103513.
(50) Ng, M.-F.; Sun, S. L.; Zhang, R. Q. *Phys. Rev. B* **2005,** *72*, 033406.
(51) Ng, M.-F.; Zhang, R. Q. *Phys. Rev. B* **2004**, *69*, 115417.
(52) Tagami, K.; Tsukada, M. *Surf. Sci.* **1997**, *384*, 308.
(53) Yu, D. K.; Zhang, R. Q.; Lee, S. T. *J. Appl. Phys.* **2002**, *92*, 7453.
(54) Bacon, A. D.; Zerner, M. C. *Theor. Chim. Acta* **1979**, *53*, 21.
(55) Polihronov, J. G.; Hedström, M.; Hummel, R. E.; Cheng, H.-P. *J. Lumin*. **2002**, *96*, 119.
(56) Horiuchi, H.; Nakano, Y.; Matsumoto, T.; Unno, M.; Matsumoto, H.; Hiratsuka, H. *Chem. Phys. Lett*. **2000**, *322*, 33.
(57) Read, A. J.; Needs, R. J.; Nash, K. J.; Canham, L. T.; Calcott, P. D. J.; Qteish, A. *Phys. Rev. Lett*. **1992**, *69*, 1232.
(58) Mitas, L.; Therrien, J.; Twesten, R.; Belomoin, G.; Nayfeh, M. H. *Appl. Phys. Lett*. **2001**, *78*, 1918.
(59) Yokojima, S.; Meier, T.; Mukamel, S. *J. Chem. Phys.* **1997**, *106*, 3837.
(60) Zhao, X.; Wei, C. M.; Yang, L.; Chou, M. Y. *Phys. Rev. Lett*. **2004**, *92*, 236805.